



Cite this: *Phys. Chem. Chem. Phys.*,
2020, 22, 12732

Highly branched triple-chain surfactant-mediated electrochemical exfoliation of graphite to obtain graphene oxide: colloidal behaviour and application in water treatment†

Nur Amirah Jamaluddin,^a Azmi Mohamed,^{id} *^{ab} Suriani Abu Bakar,^b
Tretya Ardyani,^{id} ^a Masanobu Sagisaka,^{id} ^c Shota Suhara,^c Mohamad Hafiz Mamat,^d
Mohd Khairul Ahmad,^e Stephen M. King,^{id} ^f Sarah E. Rogers^{id} ^f and Julian Eastoe^g

The generation of surfactant-assisted exfoliated graphene oxide (sEGO) by electrochemical exfoliation is influenced by the presence of surfactants, and in particular the hydrophobic tail molecular-architecture. Increasing surfactant chain branching may improve the affinity for the graphite surfaces to provide enhanced intersheet separation and stabilisation of exfoliated sheets. The resulting sEGO composites can be readily used to remove of a model pollutant, the dye, methylene blue (MB), from aqueous solutions by providing abundant sites for dye adsorption. This article explores relationships between surfactant structure and the performance of sEGO for MB adsorption. Double-branched and highly branched triple-chain graphene-compatible surfactants were successfully synthesised and characterised by ¹H NMR spectroscopy. These surfactants were used to produce sEGO via electrochemical exfoliation of graphite, and the sEGOs generated were further utilised in batch adsorption studies of MB from aqueous solutions. The properties of these synthesised surfactants were compared with those of a common single-chain standard surfactant, sodium dodecyl-sulfate (SDS). The structural morphology of sEGO was assessed using Raman spectroscopy and field emission scanning electron microscopy (FESEM). To reveal the links between the hydrophobic chain structure and the sEGO adsorption capacity, UV-visible spectroscopy, zeta potential, and air–water (a/w) surface tension measurements were conducted. The aggregation behaviour of the surfactants was studied using small-angle neutron scattering (SANS). The highly branched triple-chain surfactant sodium 1,4-bis(neopentylloxy)-3-(neopentylcarbonyl)-1,4-dioxobutane-2-sulfonate (TC14) displayed enhanced exfoliating efficiency compared to those of the single- and double-chain surfactants, leading to ~83% MB removal. The findings suggest that highly branched triple-chain surfactants are able to offer more adsorption sites, by expanding the sEGO interlayer gap for MB adsorption, compared to standard single-chain surfactants.

Received 5th March 2020,
Accepted 18th May 2020

DOI: 10.1039/d0cp01243b

rsc.li/pccp

^a Department of Chemistry, Faculty of Science and Mathematics, Universiti Pendidikan Sultan Idris, 35900 Tanjong Malim, Perak, Malaysia.
E-mail: azmi.mohamed@fsm.upsi.edu.my

^b Nanotechnology Research Centre, Faculty of Science and Mathematics, Universiti Pendidikan Sultan Idris, 35900 Tanjong Malim, Perak, Malaysia

^c Department of Frontier Materials Chemistry, Graduate School of Science and Technology, Hirosaki University, Bunkyo-cho 3, Hirosaki, Aomori 036-8561, Japan

^d NANO-ElecTronic Centre (NET), Faculty of Electrical Engineering, Universiti Teknologi MARA (UiTM), 40450 Shah Alam, Selangor, Malaysia

^e Microelectronic and Nanotechnology – Shamsuddin Research Centre (MiNT-SRC), Faculty of Electrical and Electronic Engineering, Universiti Tun Hussein Onn Malaysia, 86400 Parit Raja, Batu Pahat, Johor, Malaysia

^f ISIS Pulsed Neutron & Muon Source, STFC Rutherford Appleton Laboratory, Harwell Campus, Didcot, Oxfordshire, OX11 0QT, UK

^g School of Chemistry, University of Bristol, Cantock's Close, Bristol, BS8 1TS, UK

† Electronic supplementary information (ESI) available. See DOI: 10.1039/d0cp01243b

Introduction

Water contamination has been a major environmental issue for many years. Various contaminants, such as organic dyes,¹ heavy metals (e.g., copper and lead),^{2–4} and unwanted materials (e.g., selenium),⁵ many of which are toxic, are discharged into receiving waters, imparting undesirable colour (in the case of dyes) and health effects. Methylene blue (MB) is among the most frequent anthropogenic water contaminants, being an aromatic cationic dye that is widely used in the textile,⁶ paper and agrochemical industries.⁷ Hence, there is a pressing need to eliminate this pollutant from wastewater and find effective and economical adsorbents for water treatment.

In general, adsorption is the most favoured method for eliminating dye from aquatic environments because it is simple

and economical, offers high removal efficiency at low operational cost, generates minimal secondary by-products (e.g., sludge formation), and is able to separate a wide range of pollutants. There are various mechanisms for adsorption, such as bulk diffusion, external mass transfer, chemisorption or intraparticle diffusion.⁸ The adsorption process itself can be physical (dominated by van der Waals interactions) or chemical (ionic or covalent bonding between the adsorbate and adsorbent).⁹

Traditional carbon-based adsorbents for MB effluents, such as activated carbon (AC), have been successfully deployed for many years because they are reasonably effective and inexpensive. More recently, however, interest has been directed towards emerging advanced carbon nanomaterials, such as carbon nanotubes (CNTs),¹² and how these materials might be used in wastewater treatment. Nevertheless, AC is not always effective at removing all contaminants as it is susceptible to clogging and fouling⁷ and whilst CNTs can outperform AC, they are not yet cost-effective.^{9,10} Hence, there is a potential interest in alternative carbon-based adsorbents.

Ever since the discovery of graphene by Geim and Novoselov in 2004,¹¹ graphene-based materials have attracted substantial interest and have been evaluated for various applications.^{2–4} Recently, for wastewater treatment there has been increased focus on graphene oxide (GO).¹⁵ Since GO possesses a high surface area to mass ratio ($736.6 \text{ m}^2 \text{ g}^{-1}$)¹⁶ and includes polar oxygen functional groups, GO is strongly hydrophilic and demonstrates good dispersibility in aqueous systems.¹⁷ Being negatively charged, GO is suitable for treating wastewater containing positively charged pollutants by promoting hydrogen bonding or electrostatic interactions.⁸ The production of GO is also rather straightforward and can be performed at reasonable cost from cheap natural graphite deposits.¹⁸

As pointed out by Heard,¹⁹ the method of GO production can be tailored based on the target application. There are several methods to generate GO, including the modified Hummers' method,^{21,22} chemical vapour deposition (CVD),^{23,24} epitaxial growth,²⁴ and liquid-phase exfoliation (LPE)^{14,25} or electrochemical exfoliation of graphite.^{26–28} Among these methods, electrochemical exfoliation facilitated by surfactants, is simple and also less hazardous than the Hummers' method. The surfactants used in this process promote intercalation and exfoliation of graphite and formation of oxidised GO.²⁸ As such, surfactant-facilitated exfoliation of graphite can be considered an appealing method for graphene production.^{29–32} Electrochemical exfoliation has been explored with approaches involving sulfuric acid^{33,34} and sodium sulfate solution³⁵ as electrolytes.

The ability of surfactants to adsorb at interfaces and self-assemble as micelles is beneficial for intercalation within graphene layers^{30,31} and promotes additional GO surface area to further enhance adsorption. Although several studies have been performed,^{42,53,77} understanding about the role of adsorbed surfactant in GO production, and for the dye removal process is still quite sparse. Moreover, recent literature has mainly focused on the effectiveness and optimisation of exfoliation, where the surfactant only acts as a stabilising agent,¹⁵ rather than addressing the fundamentals of the contaminant

and dye removal process. Ideally, the goal is to develop surfactants that will simultaneously promote both efficient exfoliation and dye removal.

A previous study using ionic surfactants revealed that varying the number of surfactant chains (one, two or three surfactant tails) enhances the compatibility between graphene surfaces and surfactant molecules, facilitating improved exfoliation.³⁸ Along similar lines, in this work, the surfactants are also designed with different numbers of chains to improve their graphene compatibility. Here, the production of a few layers of graphene oxide *via* electrochemical exfoliation is investigated with added custom-made graphene-philic anionic surfactants: a double-tailed surfactant, AOT-14 (sodium bis(3,3,3-trimethyl-1-propyl)sulfosuccinate), and a triple-tailed surfactant, TC14 (sodium 1,4-bis(neopentyl-oxo)-3-(neopentylcarbonyl)-1,4-dioxobutane-2-sulfonate) (see Table 1). The term surfactant/graphene composite (sEGO) will be used throughout this article to refer to the graphene oxide materials generated in this way. To investigate the effect of surfactant chemical structure the performance of these custom-synthesised surfactants was compared with the common single-tail anionic surfactant SDS (sodium dodecylsulfate, Table 1). It was found that enhanced methylated and branched chain structures bestow enhanced adsorption capacity on these sEGO, with up to 82.7% MB removal from aqueous solutions. The results presented here indicate new possibilities for direct (*in situ*) applications of surfactant-exfoliated graphene oxides as adsorbent materials and provide a platform for the generation of future surfactants for carbon nanomaterial-based water treatments.

Materials and methods

Materials

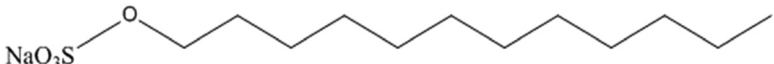
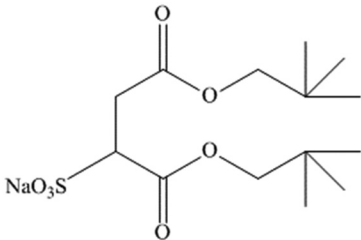
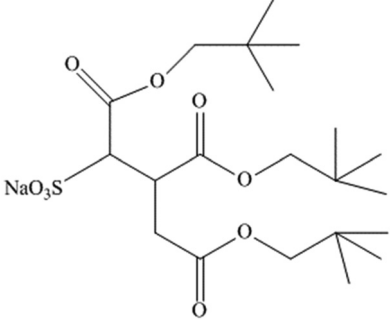
TC14 and AOT14 were synthesised as previously.^{40,41} 2,2-Dimethyl propanol (Acros, 99%) SDS (System, 99%), and deuterium oxide (Apollo Scientific Limited, 99%) were used as received. For the adsorption study, a general purpose grade of MB was purchased from Fisher Chemical and used without further purification. Detailed information regarding the surfactant characterisation is given in the ESI.†

Preparation of surfactant-assisted electrochemically exfoliated graphene oxide (sEGO)

sEGO was obtained through electrochemical exfoliation of graphite in surfactant solutions.⁴¹ Three different anionic surfactants, namely, SDS, AOT14 and TC14, were used as the electrolytes with a concentration of 0.05 M following the previous approach of Suriani *et al.*⁴¹ High-purity graphite rods (diameter 10 mm and length 15 cm, Model MV10) were used as carbon electrodes, and exfoliation was carried out for 24 h by applying a potential of 7 V to the graphite electrodes using a GW INSTEK GPS 3030DD power supply. A schematic illustration of the sEGO preparation process is presented in Fig. S3 (ESI†).

To complete exfoliation the sEGO obtained was then sonicated (Model 5510, Branson) for 1 h to generate dispersions.

Table 1 Surfactants used in this study

Surfactant name	Surfactant structure and name
SDS	 Sodium dodecylsulfate
AOT14	 Sodium 1,2-bis-(2,2-dimethyl-propoxycarbonyl)-ethanesulfonate
TC14	 Sodium 1,4-bis(neopentyloxy)-3-(neopentyloxycarbonyl)-1,4-dioxobutane-2-sulfonate

To determine the mass of sEGO in suspension, the graphite rods were weighed before and after exfoliation (refer to Table S3, ESI† for further details). It is important to note that added surfactants are crucial components for the electrolyte, as exfoliation does not occur without surfactant.

Preparation of sEGO adsorbents and dye solutions

A known amount of sEGO suspension was adjusted to neutral pH with 0.1 M NaOH and 0.1 M HCl using a Thermo Orion 2 Star pH Benchtop Meter. Dye solutions were prepared by dissolving appropriate amounts of MB in deionised water. The stock solutions were diluted to the required concentrations and adjusted to neutral pH as well (see Fig. S5, ESI†).

Adsorption of methylene blue (MB) on sEGO

Batch adsorption experiments were conducted by adding a prerequisite amount of neutral-pH MB (see Table S3, ESI†) to sEGO suspensions prepared in 250 mL Erlenmeyer flasks. The flasks containing sEGO and dye solution were sealed and shaken at a constant speed of 110 rpm using an orbital shaker (Protech Model 720). The effect of initial MB concentration in the range of 5–15 mg L⁻¹ was studied and contact time was varied from 15–1440 min. At the end of the equilibration period, 1 mL of sample was taken from the sEGO/MB dispersion and then subjected to centrifugation at 6000 rpm for 5 min. The concentration of MB in the supernatant was measured using a UV-Vis spectrophotometer (Shimadzu 1800) at λ_{max} 664 nm (optimum wavelength) with a 1 cm cuvette.

The percentage of MB removal ($R\%$) from the aqueous solution was calculated using eqn (1). Eqn (2) was used to calculate the adsorbed amount of MB.

$$R\% = \left(\frac{C_0 - C_e}{C_0} \right) \times 100 \quad (1)$$

$$q_e = \frac{(C_0 - C_e)V}{W} \quad (2)$$

where q_e is the amount of MB adsorbed per gram adsorbent (mg g⁻¹), C_0 is the initial MB concentration (mg L⁻¹), C_e is the equilibrium MB concentration (mg L⁻¹), V is the volume of solution (L) and W is the mass of adsorbent (g). The adsorption experiments were performed in triplicate. To investigate whether the presence of surfactants in sEGO may alter the adsorption process, it is instructive to measure the system with surfactant solely as an adsorbent. To provide a comparison, data were collected at similar initial concentrations to those in systems containing sEGO. An attempt to use the surfactants for MB adsorption without sEGO resulted in a negligible removal of less than 1% for all surfactants used in this study.

sEGO morphology characterization

The morphology and structure of sEGO was investigated using field emission scanning electron microscopy (FESEM, Hitachi SU8020). Raman spectra of sEGO were collected using a Renishaw InVia micro Raman spectrophotometer with a wavelength of 514 nm.

Zeta potential measurement of sEGO suspension

The colloidal stability of sEGO was assessed by determining the surface charge properties as characterized using an ELSZ-1000 zeta potential and particle size analyser (Photal OTSUKA ELECTRONICS) with the Smoluchowski equation as the zeta potential conversion equation and single-peak Lorentz fitting. Measurements were carried out in a flow cell with sampling time 400 μs , accumulation number 7, measuring angle 15° , temperature 25°C , pin hole size 50 μm , and cell constant 70.000 cm^{-1} . The properties of water (refractive index 1.3328, viscosity 0.8878 cP, and permittivity 78.3 F m^{-1}) were used for the calculation of the zeta potential. Zeta potential values were finally obtained as average values of 10 runs for each sample.

Small-angle neutron scattering measurements

The small-angle neutron scattering (SANS) experiments were performed using the time-of-flight diffractometer LOQ instrument at the ISIS Pulsed Neutron & Muon Source, UK. The accessible Q range was $0.007\text{--}0.23\text{ \AA}^{-1}$, arising from incident neutron wavelengths of $\lambda = 2.2\text{--}10\text{ \AA}$ at 25 Hz. The samples for SANS were prepared in deuterium oxide (D_2O) to enhance the neutron contrast and improve signal-to-noise, contained in 2 mm path-length quartz cells and held in a thermostatted computer-controlled sample changer at 25°C . Absolute scattering intensities $I(Q)$ (cm^{-1}) were determined to be within 5% by measuring the scattering from a partially deuterated polymer standard of known molecular weight and hence known $I(Q = 0)$. The instrument-independent reduced SANS data generated using the Mantid framework (www.mantidproject.org), were then model-fit using the SasView program (www.sasview.org) by constraining scattering length densities and other known parameters to *a priori* values. Unknown structural parameters were allowed to be refined during the fitting process to obtain an optimized fit as required by the different scattering model functions. The SANS data are presented as a function of the (magnitude of the) scattering vector, $Q = (4\pi/\lambda) \sin(\theta)$, where θ is half of the scattering angle. The approximate size of a feature is thus $2\pi/Q$.

Surface tension measurements

Air–water (a/w) surface tension values for the surfactants and sEGO were determined using a Willhelmy tensiometer (CBVP-A3, Kyowa Interface Science) equipped with a platinum plate. All measurements were taken at 25°C once the surface tension of the aqueous surfactant solutions reached equilibrium. The critical micelle concentrations (cmc) of each surfactant were determined from the intersection of the surface tension (γ) versus $\ln(\text{concentration})$ plots.

Results and discussion

Adsorption studies: effect of operating parameters

The adsorption activity (percentage dye removal and adsorption capacity) of an adsorbent is affected by various parameters, such as the initial dye concentration, contact time, solution pH, mass of adsorbent and temperature.^{7,43,44} In this work the

effect of initial dye concentration and contact time were considered for the batch adsorption analyses. Related parameters, *i.e.*, pH and mass of adsorbent, were fixed throughout. According to Haubner *et al.*,⁴⁴ a higher pH leads to weaker electrostatic interactions, which will affect dye removal; hence, a neutral pH was used. It is also known that the amount of adsorbent will significantly affect the adsorption capacity, and the optimum mass was determined to be 5 mg sEGO. For reference, the relationships between percentage removal and mass of adsorbent are given in the ESI† (Fig. S6). Experiments were conducted at an optimum temperature, which was found to be 22.5°C (Fig. S7, ESI†). Previous studies have mainly focused on finding an adsorbent that provides the highest percentage of dye removal and adsorption capacity.^{6,7} This current study investigates the effects of surfactant tail structure variations on the preparation of sEGO for dye removal in aqueous applications.

Effect of initial dye concentration

Differences in dye adsorption capacity and initial dye concentration have been probed by studies as a function of dye concentration. It was found that more than 50% removal could be achieved by AOT14 sEGO and TC14 sEGO at 7, 10, 13 and 15 ppm MB, in contrast to SDS sEGO (see Fig. 1a). The significant removal achieved at such a high initial concentration of MB (15 ppm) may be attributed to the high ratio of active binding sites to the number of MB molecules, resulting

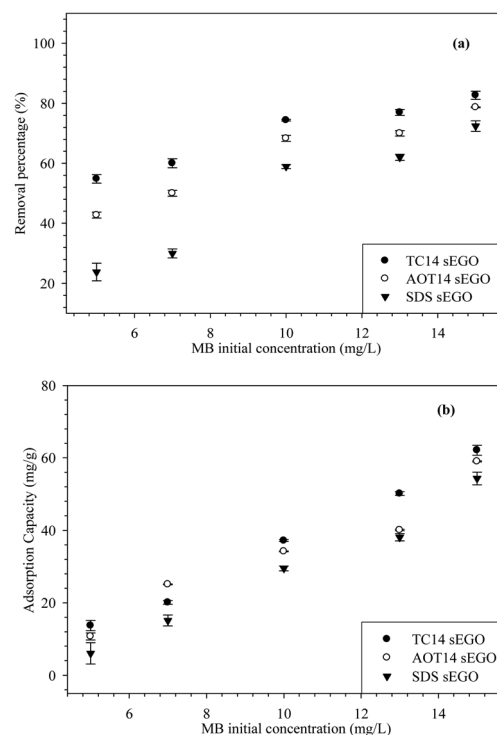


Fig. 1 The percentage removal (a) and adsorption capacity (b) of MB from aqueous dispersion by sEGO containing surfactants at equilibrium dye concentrations with 24 hours contact time. The error bar represents the standard deviation ($n = 3$).

Table 2 Comparison of the adsorption capacities of various reported graphene-based adsorbents for MB

Adsorbent	Source & method	Adsorbent dosage (mg)	Removal percentage (%)	Adsorption capacity (mg g ⁻¹)	Initial dye concentration (ppm)	pH	Temperature	Contact time (min)	Ref.
TC14 sEGO	Electrochemical graphite	5	82.7	62.1	5–15	7	23 °C	1440	This study
AOT14 sEGO	exfoliation & <i>in situ</i> method	5	73.9	55.5	5–15	7	23 °C	1440	This study
SDS sEGO		5	72.4	54.3	5–15	7	23 °C	1440	This study
SDS-exfoliated graphene	Ultrasonic exfoliation of graphite & dispersion	1.1	86.5	782.3	10, 50 and 100	3–9	25 °C	2880	15
Exfoliated graphene oxide (EGO)	Modified Hummers & dispersion	11	95	—	40	6	—	160	42
Exfoliated graphene	Graphite exfoliation & freeze dried	10	105	511.70	500	6	Room temperature	60	35
Graphene	Modified Hummers & dispersion	20–170	—	153.85	20–120	3–10	293 K	0–1500	46
Graphene oxide (GO)	Modified Hummers & dispersion	25	98	243.90	40–120	6	—	0–350	45
Carbon nanotubes (CNT)	Ni nanoparticle-catalysed pyrolysis	25	75	188.68	40–120	6	—	0–350	45
Activated carbon (AC)	<i>Enteromorpha prolifera</i> by zinc chloride activation	25	100	270.27	40–120	6	—	0–350	45

in good adsorbent–adsorbate interactions.⁴⁵ However, at lower initial concentrations of dye (5, 7 and 10 ppm), the removal efficiency decreased, suggesting saturation of adsorption sites on the adsorbent by competing adsorbate molecules.⁴⁵

MB adsorption onto sEGO reached 72.4% ± 1.8, 73.9% ± 0.2 and 82.7% ± 1.4 for SDS, AOT14 and TC14 sEGO, respectively, at 15 ppm MB. The adsorption capacity at this dye concentration was 62.1 mg g⁻¹ for TC14 sEGO, compared to 55.5 mg g⁻¹ for AOT14 sEGO and 54.3 mg g⁻¹ for SDS sEGO (see Fig. 1). These results are particularly interesting considering that these sEGO nanomaterials can be easily produced compared other approaches (see Table 2).

The expansion of the graphite layers³⁶ was mainly caused by the current supply (from the voltammeter)⁸⁰ along with micelle formation and individual surfactant (monomer) activity, whereby these two entities were responsible for the intercalation process. The enhanced performance of TC14 sEGO is attributed to its ability to form micelles, facilitating more GO surface area through expansion of the graphite layers³⁶ by micelle formation. The presence of surfactant layers on the GO surfaces will also increase the overall negative surface charge. Surface adsorbed surfactant molecules can also function as stabilisers, preventing the agglomeration of sEGO by weakening the π - π stacking interactions. Hence, these sEGO materials have higher specific surface areas and numbers of accessible adsorbent sites.¹⁵

Effect of contact time

To gauge the optimum equilibration time, dye ion binding was studied for contact times from 15–1440 min (24 hours). Samples were taken after 15 min for the first reading to allow the adsorption process to occur. The time profile of MB adsorption is depicted in Fig. S8 (ESI†). In general, there are two stages: rapid adsorption and then a gradual increase until equilibrium is reached. A high degree of MB (at 15 ppm) removal was achieved within the first hour of contact for TC14 sEGO (82.7%), whereas AOT14 sEGO and SDS sEGO showed removal of 78.7 and 74.7%, respectively. The initially high degree of MB adsorption indicates essentially instantaneous adsorption, which in turn points to a surfeit of binding sites on

sEGO. Prolonging the contact time showed no obvious increase in removal, implying attainment of equilibrium: either all the active sites had become saturated, or there were no more MB molecules to adsorb. The results imply that a contact time of 24 hours was more than adequate to achieve saturated adsorption of MB onto all sEGO adsorbents. The removal of MB was analysed at particular intervals between 15 min and 24 hours is shown in Fig. S8 (ESI†), and as can be seen, after approximately 6 hours the percentage removal remained constant.^{5,6}

Adsorption isotherms

Adsorption isotherm models have been used to describe the adsorption capacities as well as the distribution of MB between the solid and liquid phases at equilibrium.⁴⁷ The Langmuir and Freundlich isotherm models were employed to fit the equilibrium adsorption data. The Langmuir isotherm (eqn (3)) is based on the assumption that adsorption leads to a monolayer coverage of adsorbate on a homogenous adsorbent surface with a finite number of adsorption sites.⁴⁸

$$\frac{q_e}{C_e} = K_L Q_0 - K_L q_e \quad (3)$$

where C_e is the equilibrium concentration of MB (mg L⁻¹), q_e is the equilibrium amount of MB ions adsorbed on the adsorbent (mg g⁻¹), K_L is the Langmuir constant (L mg⁻¹), and Q_0 is the maximum monolayer coverage capacity (mg g⁻¹). The significant feature of the Langmuir isotherm is expressed in terms of a dimensionless factor (R_L) as defined in eqn (4), which characterizes the favourability of adsorption ($0 \leq R_L \leq 1$).

$$R_L = \frac{1}{1 + K_L C_0} \quad (4)$$

In contrast, the Freundlich isotherm model considers multi-layer adsorption on a heterogeneous surface.⁴⁹ The linear form of the Freundlich isotherm is expressed in eqn (5)

$$\log q_e = \frac{1}{n} \log C_e + \log K_F \quad (5)$$

where n and K_F are the Freundlich parameters and the other quantities have the meanings described above. A linear plot of $\log q_e$ against $\log C_e$ gives K_F and n . The Langmuir and Freundlich isotherm plots are shown in Fig. S9a and b, respectively (ESI[†]), and the calculated parameters from both isotherms are summarized in Table S4 (ESI[†]).

As shown in Table S4 (ESI[†]), the adsorption of MB into TC14 sEGO is well described by a Langmuir model with a correlation coefficient (R^2) of 0.99. Either a Freundlich or Langmuir isotherm can be used to describe the adsorption of MB by AOT14 sEGO and SDS sEGO (R^2 is close to 0.9 or 1). These results therefore suggest that all the sEGO surfaces studied act as either homogenous or heterogeneous adsorbents and adsorption resulted in either monolayer or multilayer coverage in the presence of defects (carboxyl, hydroxyl and epoxy functional groups on sEGO layers).

The adsorption behaviour of MB ions onto sEGO surfaces can be further evaluated through a dimensionless constant, the separation factor (R_L), indicating the favourability of adsorption: favourable when $R_L = 0$, unfavourable when $R_L > 1$ and linear when $R_L = 1^2$. Since all the R_L values are in the range between 0 and 1 (0.15 for TC14 sEGO, 0.18 for AOT14 sEGO and 0.22 for SDS sEGO), adsorption is apparently favourable. In the Freundlich isotherm model, adsorbent heterogeneity is indicated by an n value approaching zero.² For each of TC14 sEGO, AOT14 sEGO and SDS sEGO n was found to be close to zero, 0.11, 0.07 and 0.04, respectively. Thus, it can be concluded that adsorption can be well described by both Langmuir and Freundlich adsorption isotherms.

Adsorption kinetics

To determine the rate of adsorption and the mechanism controlling the adsorption process, pseudo-first- and pseudo-second-order kinetic models were investigated.^{50,51} It is of interest to understand whether the adsorption involves physisorption (pseudo-first-order kinetic model) or chemisorption (second-order kinetic model). The equations^{50,53} representing these models are

$$\log(q_e - q_t) = \log q_e - \frac{k_1}{2.303}t \quad (6)$$

$$\frac{t}{q_t} = \frac{1}{k_2 q_e^2} + \frac{t}{q_e} \quad (7)$$

Here, q_e and q_t are the adsorption capacities at equilibrium and at time t , respectively. k_1 (min^{-1}) and k_2 ($\text{g mg}^{-1} \text{min}^{-1}$) are the rate constants for the pseudo-first- and pseudo-second-order rate laws. The plots of $\log(q_e - q_t)$ and t/q_t against t for MB adsorption at fixed concentrations were linear (Fig. S10, ESI[†]), and the calculated values of k_2 , q_e and R^2 are summarized in Table S4 (ESI[†]). The results demonstrate that the pseudo-second-order model performs well ($R^2 > 0.99$), which is characteristic of chemisorption. MB is a cationic planar dye molecule with possibilities for π - π stacking of aromatic rings to provide dipolar interactions with surfactant sEGOs containing hydroxyl, epoxide and carboxyl functional groups.⁵² Montes-Navajaz *et al.*,¹⁶

proposed that MB ($\text{p}K_a = 3.14$) protonation plays a significant role in the adsorption of MB molecules onto sEGO adsorbents, whereby conjugation between MB and the sEGO surfaces occurs¹⁶ since MB consists of sulfur and stabilized nitrogen atoms in a conjugated system.

Observations of sEGO in aqueous solutions

The morphological features of the sEGOs were observed using FESEM. From the FESEM micrograph in Fig. 2, it can be seen that the surface morphology of sEGO exists as a folded and disorderly sheet-like structure, which is typical for graphene oxide.⁵³ The FESEM results for exfoliated graphene were similar to those for GO produced through the Hummers' method:⁴² the carbon material surfaces displayed ripples and obvious layers, which are distinctive features of graphene and GO. Along with the stacked layers of sEGO, the relatively smooth, compact structure and puffy nature of sEGO can also be seen, which is due to the interaction of various oxygen-containing functional groups⁵⁴ originating from the surfactant headgroups. The material with TC14 sEGO has a more expanded structure than for AOT14 sEGO and SDS sEGO. This difference indicates that the TC14 sEGO surface may be richer in oxygenated groups such as hydroxyl, carboxyl, epoxy and carbonyl groups. The FESEM analysis suggests that the surfactants were uniformly embedded between the stacked layers of GO, thereby helping to prevent agglomeration of the GO sheets.⁵⁵ This leads to an increase in effective surface area of sEGOs, which in turn, leads to enhancement of the MB adsorption. Under high magnification imaging (Fig. 2a'-c'), there is evidence that the GO sheets still exist as exfoliated thin layers, again confirming that the presence of surfactants helps weaken the van der Waals interactions between adjacent GO sheets. The surfactants are presumed to strongly adsorb onto the GO sheets through electrostatic interactions with the oxygen-containing moieties. In addition to being effective as dispersants, surfactants may enhance the adsorption of MB on sEGO surfaces. Unfortunately, a comparison with GO without surfactant cannot be made here, as the exfoliation process requires a charged electrolyte.

Raman spectroscopy

Structural defects in graphenes, *e.g.*, oxides,⁵³ can be investigated with Raman spectroscopy, helping indicate the formation of sEGO. According to Lotya *et al.*,⁵³ the characteristic peaks of carbon nanomaterials lie at approximately 1350 cm^{-1} and 1582 cm^{-1} , which represent the D band and G band, respectively. Hao *et al.*,⁵⁶ stated that a higher peak intensity of the G band at approximately 1580 cm^{-1} indicates a greater number of layers due to the presence of more carbon atoms. A broadened G band with increasing D band intensity is attributed to the effect of exfoliation, which leads to a decrease in the in-plane sp^2 bonding of the graphene.¹³ On the other hand, the presence of the D band is related to the existence of hydroxyl, epoxy and carboxyl functional groups on the graphene layers and can be used to monitor the oxidation process.⁵⁷

Fig. 3 presents the Raman spectra of graphite, TC14 sEGO, AOT14 sEGO and SDS sEGO. Prior to exfoliation, the D band of

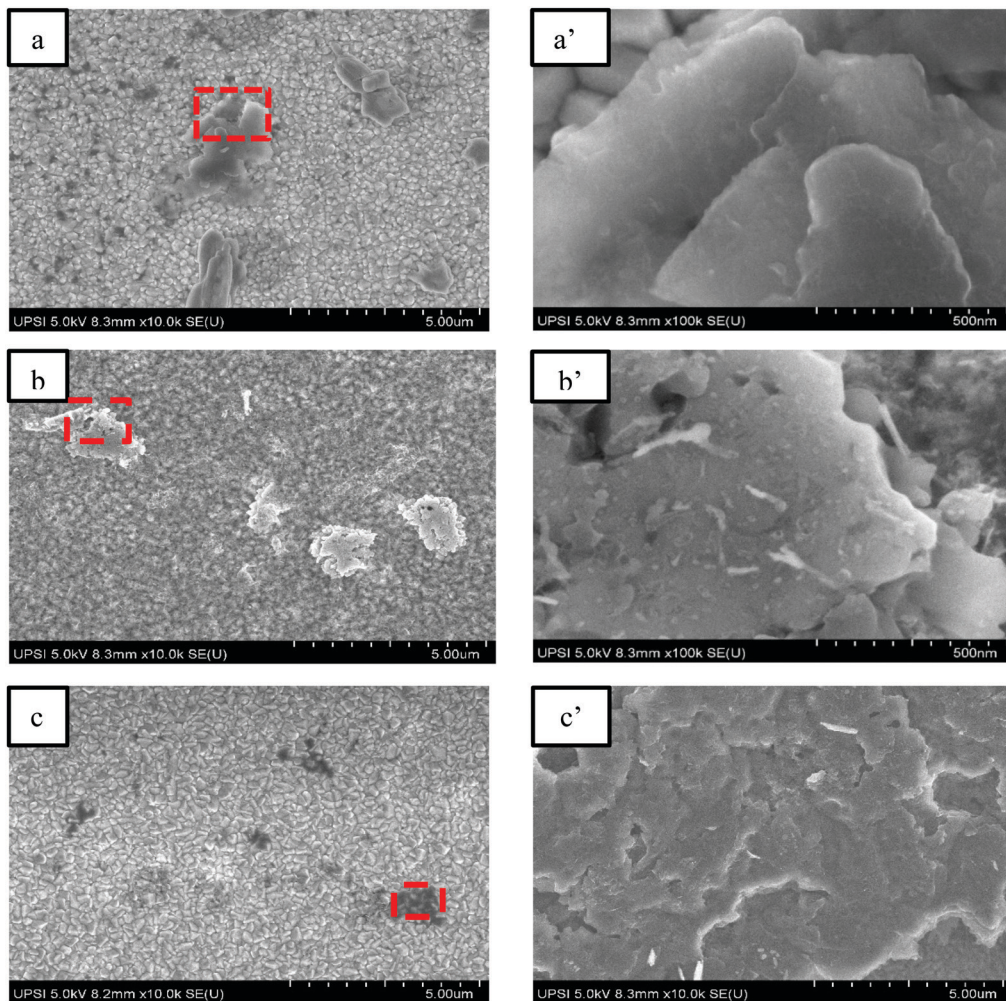


Fig. 2 FESEM images of SDS sEGO (a and a'), AOT14 sEGO (b and b') and TC14 sEGO (c and c').

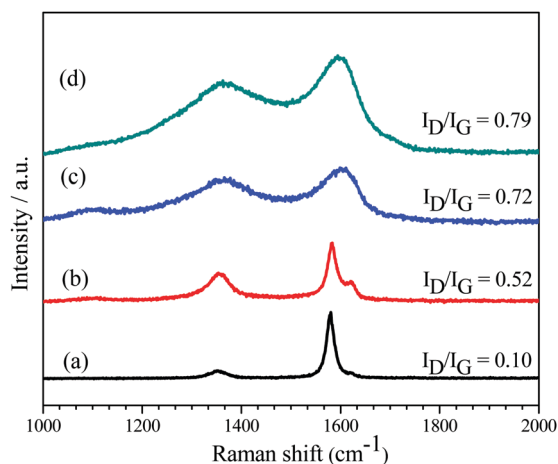


Fig. 3 Raman spectra of graphite (a), SDS sEGO (b), AOT14 sEGO (c), and TC14 sEGO (d).

graphite is negligible compared to the strong G band, indicating small defects and the preservation of the sp² character of the honeycomb network. In all the sEGO samples exfoliation

transforms the appearance of the D bands at 1363 cm⁻¹: they are broad and strong, confirming oxidation and an evolution of sp² into sp³ owing to the introduction of oxygen-containing functional groups.⁵⁸ In addition to enhancing the D band, oxidation leads to notable G band intensities at 1583, 1595 and 1611 cm⁻¹ for SDS sEGO, AOT14 sEGO and TC14 sEGO, respectively, compared to that at 1580 cm⁻¹ in pristine graphite.

These peaks correspond to the E_{2g} vibrational mode occurring in the aromatic carbon rings. In addition, the G bands of the AOT14 and TC14 sEGOs are broader than for graphite, which may indicate that after exfoliation, the structural symmetry decreases along with an increase in vibration modes from destruction of C=C bonds.⁵³ The significant G band Raman shift for TC14 sEGO is likely due to an increase in GO layers.⁵⁹ The higher wavenumber of the G band and the full width half maximum (FWHM) for all sEGOs compared to those of pristine graphite indicate the presence of oxygen.⁷⁹ The FWHM (of the G band) was found to be 25 cm⁻¹, 38 cm⁻¹, 63 cm⁻¹ and 75 cm⁻¹ for graphite, SDS sEGO, AOT14 sEGO and TC14 sEGO, respectively, suggesting an increase in oxidation level with higher levels of sp³ carbons.⁷⁹

In addition, calculating the intensity ratio between the D (I_D) and G bands (I_G) gives an idea of the defect content and the extent of oxidation.⁵⁹ Since the hexagonal lattice of C–C graphene and graphene oxide depends on the hydrogen content based on the connection of sp^2 and sp^3 linkages, the I_D/I_G ratio is sufficient to provide proof for sEGO.⁸⁰ As a result, samples with higher I_D/I_G values will have higher degrees of disorder and more defects.⁶⁰ Analysis reveals that the graphite starting material presents very low I_D/I_G (0.10), suggesting high sp^2 structural integrity with low levels of basal and edge defects. Moreover, the sEGO samples all show a significant change in the number of defects compared to that in bulk graphite, with I_D/I_G values of 0.52, 0.72, and 0.79 for SDS sEGO, AOT14 sEGO & TC14 sEGO, respectively.

Approximation of the oxygen content in sEGO was obtained using UV-visible spectra (Fig. S11, ESI†). By comparison with literature,²⁰ the estimated oxygen contents for TC14 sEGO, AOT14 sEGO and SDS sEGO were 45%, 42% and 21%, respectively. With these results, it is fair to say that the electrochemical exfoliation process assisted by surfactants has successfully peeled graphene layers from bulk graphite and oxidized it to form graphene oxide. The oxygen-functionalized moieties on GO then play an important role in promoting the adsorption of MB molecules by the sEGO surfaces.

Zeta potential measurements

The zeta (ζ) potential is an important parameter used to describe the electrical potential or surface charge of colloidal particles^{63,65} such as sEGOs. Smith *et al.*,⁶³ noted that the height of the electrical potential energy barrier provided by adsorbed surfactant both mitigated the aggregation graphene materials and controlled the level of dispersion of graphene in the aqueous phase, generating stable systems. The stabilisation of sEGO is due to repulsions between neighbouring surfactant-coated sheets arising from the electrostatic interactions imparted by the dissociated surfactant head-groups.^{61–64} According to Johnson, Dobson and Coleman,⁶⁶ a high ζ denotes a large number of surface charges. For ionic surfactants, the sign of the zeta potential also reflects the charge and type of the adsorbed surfactant on top of the nanomaterial surface.³⁶ A $|\zeta|$ value in excess of 30 mV is generally considered to be the threshold for dispersion stability in aqueous systems.^{23,24}

To assess the effect of the surfactant on sEGO dispersions, data from a GO dispersion without surfactant taken from the literature⁶⁷ are included as a reference. The measured zeta potentials of the sEGO in this study are summarized in Table S5 (ESI†). Native GO has a ζ -20 ± 1 mV, which arises from the presence of surface carboxylate groups.⁶⁸ Interestingly, the presence of surfactant leads to larger negative potentials, implying that GO suspensions with surfactant are more stable than those without. However, within experimental error, the value for SDS sEGO is very similar to that for native GO, indicating that the linear-chain surfactant was unable to stabilize the sEGO colloids as well as the custom-made branched surfactants. With a ζ value of -46 mV, TC14 sEGO clearly has good stability beyond the threshold value⁶⁹ and outperformed both AOT14 sEGO (-29 mV) and SDS sEGO (-21 mV). It is apparent that there is a trend of increasing stability (*i.e.*, zeta

potential value) upon increasing the number of surfactant hydrophobic tails. The reason might be a higher surfactant chain branching and methylation offer improved barriers and hence higher dispersion stability. It is therefore evident that the surfactant structure, particularly the architecture of the hydrophobic tails, is key to achieving stable suspensions.

Regarding sEGO adsorption properties, it is also clear that there is a trend towards greater MB removal as the degree of chain branching is increased. This suggests that the level of adsorbed MB is linked to stability, and more negative ζ . As indicated in Table S5 (ESI†), the most stable system, TC14 sEGO, showed the highest removal (82.7%) with an adsorption capacity of 62.1 mg g^{-1} . In addition to ensuring the stability of sEGO in water, the presence of surfactant leads to a more negative overall charge, hence improving electrostatic interactions between sEGO and MB, thereby conferring dual benefits.

To further support the zeta potential data, all sEGO samples were analysed by UV-visible spectroscopy, and the results are given in the ESI.† According to Marcano *et al.*,⁷⁸ the degree of oxidation can be deduced based on the UV-visible spectrum, where absorbance is proportional to the level of oxygenated groups, which goes in hand with more negative zeta potentials (more colloiddally stable) in the sEGO system.

Surface tension measurements

The surfactant chain structure, such as length, aromatization, branching and methylation, plays a major role in the physico-chemical properties, including adsorption, micellization and cmc.⁵⁵ Here, surface tension data also show shifts in cmc after the formation sEGO systems.

Fig. 4 and Table 3 show surface tension data for SDS, AOT14, and TC14, and their corresponding sEGOs. There are sharp breaks at the cmcs, suggesting the high purity of the synthesised surfactants.³⁹ The most highly branched surfactant, TC14, exhibits a cmc of 18.0 mM, followed by double-chain AOT14 (11.0 mM) and single-chain SDS (6.7 mM). Commonly, for a homologous surfactant series an increase in tail carbon number usually leads to a logarithmic decrease in cmc.^{40,73} However, comparisons between different series of surfactants are not always so straightforward.⁷¹

Another important parameter for characterizing surfactant performance is the limiting surface tension (γ_{cmc}), representing the effectiveness of any given surfactant for achieving a maximum surface tension reduction.^{38,70,72} TC14 has the lowest γ_{cmc} value, linked to a low cohesive energy density⁷⁴ between the hydrocarbon chains, leading to easier wetting.

Pre-cmc surface tensions can provide estimations of surface excesses, Γ , and limiting head-group areas at the cmc, A_{cmc} ,^{39,74} by applying the Gibbs equation (eqn (8)), whereby m is a prefactor for dissociating 1:1 ionic surfactants = 2. In this way, it is possible to distinguish the molecular packing efficiency in the adsorbed monolayers. Table 3 shows the estimated A_{cmc} calculated using eqn (9).

$$\Gamma = -\frac{1}{mRT} \frac{d\gamma}{\ln c} \quad (8)$$

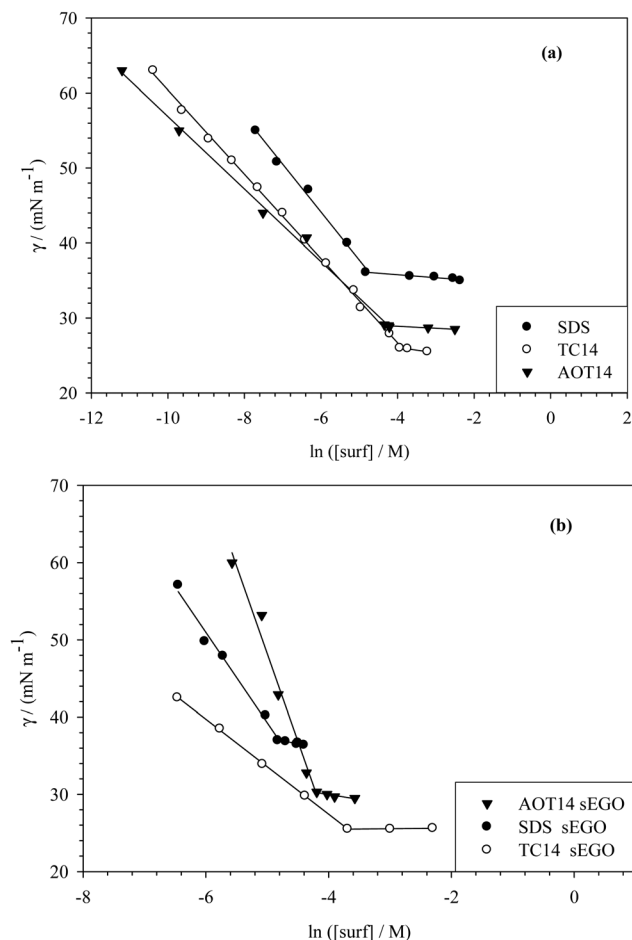


Fig. 4 Air–water surface tension γ_{cmc} vs. $\ln(\text{concentration})$ plots for aqueous solutions of surfactants (a) and sEGOs (b) at 25 °C.

Table 3 Parameters derived from surface tension measurements including the fractional free volume (FFV)

Surfactant	cmc (mM) ± 0.03	γ_{cmc} (mN m ⁻¹) ± 1	$A_{\text{cmc}}/\text{\AA}^2 \pm 2$	FFV
TC14	18.0	25.8	144	0.12
TC14 sEGO	24.7	26.0	132	0.17
AOT14	11.0	28.1	80	0.19
AOT14 sEGO	15.0	30.3	64	0.30
SDS	6.7	36.1	70	0.31
SDS sEGO	8.2	37.0	61	0.37

$$A_{\text{cmc}} = \frac{1}{\Gamma Na} \quad (9)$$

The value of A_{cmc} was found to be much higher for TC14 (144 \AA^2) and TC14 sEGO (132 \AA^2) than for the other surfactants and their corresponding sEGOs. A similar observation was previously reported by Czajka *et al.*,⁷⁵ who noted an increase in A_{cmc} of the order of 10–20 \AA^2 for branched surfactants compared to straight-chain analogues. The steric effects of the additional chain and also branching in TC14 drives the A_{cmc} higher giving high surface coverages.³⁹ Even when GO is present A_{cmc} for triple-branched TC14 is still higher than those of the rest of the series. It can be seen, however, that there are

slight decreases in A_{cmc} in the presence of GO (outside the experimental error), suggesting that the surfactants may adsorb on the sEGO layers. Such behaviour was previously noted by Mohamed *et al.*, whereby a decrease in A_{cmc} indicated less crowding of head-groups at the interface (perhaps due to reduced repulsive interactions).³⁹ This leads to the suggestion that when GO is present, a small fraction of the surfactant molecules at the interface move and adsorb on GO, which leads to weaker head-group repulsions. Further support for this conclusion comes from the micellar sizes obtained by SANS, described below.

Having established that surfactant adsorption on GO is important for the promotion of dye adsorption by sEGO, the effect of surfactant structure will now be considered. The fractional free volume (FFV) is a useful parameter in this respect, since it quantifies ‘‘bulkiness’’ of the surfactant architecture. This FFV concept was first introduced by Johnston,⁷⁶ who proposed that surface coverage and tail geometry are linked to interface stability; a lower FFV value represents better stability. The FFV values for the systems studied here calculated according to eqn (10) are listed in Table 3, where V_t is the surfactant tail volume and t_1 is the tail length of the surfactant (considering the C and H count).

$$\text{FFV} = 1 - \frac{V_t}{t_1 A_{\text{cmc}}} \quad (10)$$

The calculated FFV values decrease with tail structure, *i.e.* increased methyl groups and degree of branching. A previous study⁷⁴ using branched surfactants also showed that including chain branching in the tail structure lowered γ_{cmc} compared to those of less branched and more linear analogues. The highly branched surfactant TC14 (which is bulkier than AOT14 and SDS) caused an increase in interfacial activity, lowering the interfacial tension and leading to lower FFV values.⁷⁶

Small-angle neutron scattering

The adsorption of surfactant on nanomaterial surfaces, forming surface micelles, is known to play a crucial role in determining stability.⁵⁵ For this reason, a general picture of micelle formation by surfactants for dispersing and stabilizing sEGO is therefore useful to understand structure and interactions. An ideal technique for studying surfactant micellization is small-angle neutron scattering (SANS).

Fig. 5 displays the SANS data for solutions of the surfactants used in this study (SDS, AOT, and TC14) and the respective sEGO suspensions for comparison. The parameters obtained from fitting the SANS data are provided in Table 4. According to Stone *et al.*,⁷⁶ the shape, volume and contrast of the nanoscale structures were assessed from the scattering intensities $I(Q)$. Over the Q range in Fig. 5a, there are minor changes in $I(Q)$ for TC14 sEGO compared to that of TC14 (at the cmc), consistent with a smaller micelle size, based on judgement by Mc Coy *et al.*⁷⁷ The small increase in $I(Q)$ in the low Q region can be interpreted as a result of surfactant adsorption indicative of sEGO formation. To further support this statement, TC14 sEGOs produced using TC14 at a lower cmc were analysed and demonstrated the absence of structured materials.

The lack of obvious changes in the AOT14 and AOT14 sEGO $I(Q)$ profiles indicate bulk micelle formation. However, a bump appears in the pure SDS solution plot compared to that of SDS sEGO, which can be assumed to arise from an increase in intermicellar interactions. There is also a bump in the profile for the AOT14 solution, but this is less prominent with added sEGO, as indicated by fitting the Hayter–Penfold charge repulsion $S(Q)$. SANS data for each individual surfactant and its corresponding sEGO for comparison can be found in Fig. 5.

The scattering from SDS is characteristic of approximately spherical but charged micelles with a radius of 22.0 Å, in accordance with previous studies.^{32–34} The shape and size of the micelles remain essentially unchanged when sEGO is formed, consistent with previous findings.³⁶ The same reasoning applies to AOT14 and TC14, where both profiles could be fitted to paracrystalline lamellar stack and ellipsoid models, respectively, with the micelle characteristics remaining in the sEGO system. These findings were also proven by previous research performed by Ardyani *et al.*,³² in which graphene oxide was invisible or ‘contrast-matched’ since there were no distinct changes in scattering. SANS data provide structural information, but not explicit adsorption mechanisms; however, GO could act as an aqueous adsorbent on the basis of the differences in scattering between the sEGO composite and pure surfactants.⁷⁷

Proposed adsorption and exfoliation mechanism

Previous studies⁸⁰ suggested a two-step exfoliation mechanism, whereby first, the formation of nucleophilic hydroxyl ions (OH^-) through aqueous reduction created in the electrolyte (in this case, surfactant solution) occurs at the graphite edges. Next, oxidation generated graphite layer expansion takes place, which then assists sulfate ion (SO_4^{2-}) intercalation between the graphite sheets. Co-intercalation between SO_4^{2-} and water might also have occurred during this stage. Generally, the current flow produced during the electrochemical exfoliation process causes surfactant ion interactions between the graphite layers in the graphite rods.³⁶ Li *et al.*,⁸¹ found that the use of an electrolyte for the electrical exfoliation of graphite made using commercial sodium dodecylbenzene sulfonate (SDBS) would result in intercalation and stabilise the colloidal environment (dual role function). For that reason, we showed here that for such a small surfactant molecule, the exfoliation efficiency can be controlled by surfactant chemical structure. Increasing the degree of the surfactant hydrophobic chain has been shown to improve the exfoliation efficiency^{32,36,37} as well as the adsorption capacity/dye uptake during batch adsorption studies.

Combining the aforementioned research with the current results, we propose how to adapt the structure of surfactants to promote both efficient exfoliation and adsorption. Previous studies have successfully used this strategy to tailor graphene compatibility.⁴⁰ Now, with growing attention to these systems it is of interest to know which combination of graphene and surfactants for generating sEGO will be most effective for a potential MB scavengers. The previous discussions on sEGO morphologies and properties based on FESEM, Raman spectroscopy, zeta potential measurements, micellar sizes and shapes

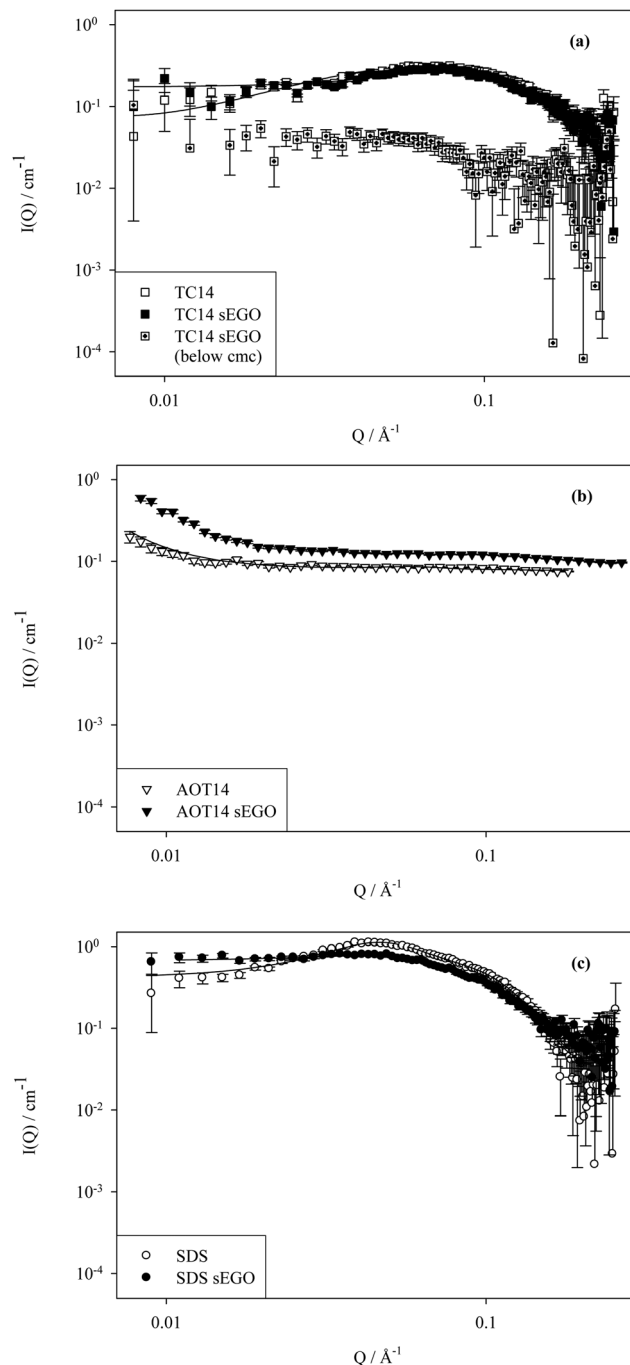


Fig. 5 SANS data for (a) TC14, TC14 sEGO and TC14 sEGO (below cmc), (b) AOT14 and AOT14 sEGO, (c) SDS and SDS sEGO. [Surfactant] = 30 mM (at cmc), while [surfactant] = 0.75 mM (below cmc); [sEGO] = 0.2 mg mL⁻¹ at $T = 25$ °C. Lines are model fits for spherical, paracrystalline lamellar stacked and ellipsoidal micelles (incorporating a Hayter–Penfold $S(Q)$). Characteristic error bars are shown for the lowest intensity samples.

using SANS, and surface tension measurements were interpreted in terms of adsorption of surfactant ions which charge the graphene layers,⁶⁷ hence in turn providing adsorption sites for MB.

Thus, the proposed exfoliation mechanism is presented in Fig. 6. Electrochemical exfoliation takes place by surfactant intercalation between graphite rod electrode layers (7 V power

Table 4 Model fit parameters for the SANS data

Sample	Model	R_{sphere} (Å)	R_a^a (Å)	R_b^b (Å)	X^c	L^d	D^d	M^d
Surfactant solution								
SDS	Sphere	22.0	—	—	—	—	—	—
AOT14	Paracrystalline lamellar stack	—	—	—	—	6.0	90.0	27.0
TC14	Ellipsoid	—	10.0	20.4	2.0	—	—	—
sEGO								
SDS sEGO	Sphere	24.0	—	—	—	—	—	—
AOT14 sEGO	Paracrystalline lamellar stack	—	—	—	—	9.0	61.0	484.0
TC14 sEGO	Ellipsoid	—	8.0	23.0	2.9	—	—	—

^a Polar radius. ^b Equatorial radius. ^c $X = R_b/R_a$. ^d For lamellar only, where L = thickness of bilayers; D = space between bilayers; and M = number of bilayers.

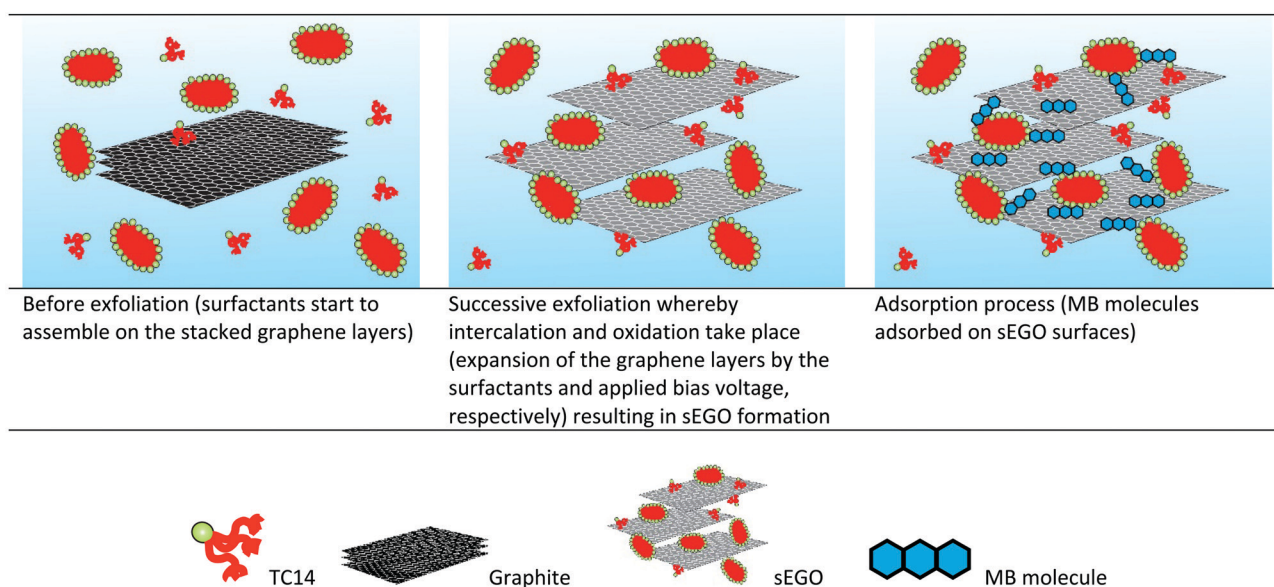


Fig. 6 Schematic representation, not to scale, of surfactant-mediated graphene exfoliation to form sEGO and the uptake of methylene blue by sEGO.

supply employed for 24 hours).³⁶ The graphite edge sheets open up through the applied bias voltage and prepared electrolyte (surfactant solution),⁸⁰ whereby the triple-chain surfactant TC14 enters the interlayer spacing. Further sEGO expansion occurs under ultrasonication.^{36,42}

The simple geometric parameter fraction free volume (FFV) is also useful for understanding the behaviour of these systems. As mentioned before, based on FFV, the effective TC14 molecular size is lower (FFV 0.12) than that of TC14 sEGO (FFV 0.17), indicating a greater efficiency for filling space. Consistent with this property, the highly branched triple-chain TC14 surfactant tail adsorbs onto the graphene sheets more effectively (whilst the head-group resides in the aqueous phase), as compared to double-chain AOT14 (FFV = 0.19) and single-chain SDS (FFV = 0.31), with FFV values for AOT14 sEGO and SDS sEGO of 0.30 and 0.37, respectively. During the exfoliation process, it is suggested that surfactant ions expand the graphene layers, hence forming sEGO composites.

The fundamental mechanisms controlling MB adsorption on the sEGO surface at pH 7 include (i) electrostatic interactions

between the positively charged N^+ groups of MB and the inherently negatively charged sEGO (from the $-O_3S^-$ in the surfactant head-group), (ii) π - π stacking interactions between sEGO layers by the MB aromatic rings and (iii) hydrophobic interactions between hydrophobic parts of MB (benzyl groups) and hydrophobic parts of surfactant sEGOs ($-CH_3$ and $-CH_2-$ groups and hydrocarbon tails). Although the adsorption capacity of MB from aqueous solution has been proven through batch experiments, just how much of the adsorption was due to binding of MB to the surfactant is hard to evaluate. Further studies on this issue are required.

Conclusions

In this work, surfactant chain structure and branching^{40,73} were proven to affect interactions,³² thereby tailoring the structures and properties of surfactant-graphene oxide composites (sEGOs). The structural changes induced by surfactant type also affect the capacity and effectiveness of the sEGOs as

adsorbents for the model pollutant dye methylene blue (MB). It was found that a highly branched tri-chain surfactant, TC14, conferred TC14 sEGOs with a much higher adsorption capacity than composites generated with a common linear single-chain compound SDS. This shows that surfactant design can beneficially affect the properties of exfoliated sEGOs, paving the way for tailored improvements in applications of these systems as adsorbents for aqueous pollutants. Although the adsorption and removal capacities shown here were not as high as those of some other carbon nanoadsorbents,^{16,43,46,47,49} there are other advantages, especially a much more straightforward exfoliation and production process. As such, the approach described here opens up new avenues for the wider applications of sEGOs, in for example in wastewater treatment.

Conflicts of interest

There are no conflicts to declare.

Acknowledgements

This work was funded under a grant from Universiti Pendidikan Sultan Idris Rising Star Research Grant (Grant Code: 2019-0118-103-01). This project was also supported by JSPS [KAKENHI, Grant-in-Aid for Young Scientists (A), No 23685034] and Leading Research Organizations (RCUK [through EPSRC EP/I018301/1], ANR[13-G8ME0003]) under the G8 Research Councils Initiative for Multi-lateral Research Funding—G8-2012. The authors thank the Science and Technology Facilities Council for the allocation of beam time, travel and consumables (experiment number RB1710004). This work benefited from the use of the SasView application, originally developed under NSF Award DMR-0520547. SasView also contains code developed with funding from the EU Horizon 2020 programme under the SINE2020 project Grant No. 654000.

Notes and references

- S. Song, Y. Ma, H. Shen, M. Zhang and Z. Zhang, *RSC Adv.*, 2015, **5**, 27922–27932.
- A. B. Albadarin, J. Mo, Y. Glocheux, S. Allen, G. Walker and C. Mangwandi, *Chem. Eng. J.*, 2014, **255**, 525–534.
- M. Ghaedi, H. Mazaheri, S. Khodadoust, S. Hajati and M. K. Purkait, *Spectrochim. Acta, Part A*, 2015, **135**, 479–490.
- X. Wang, Y. Liu, H. Pang, S. Yu, Y. Ai, X. Ma, G. Song, T. Hayat, A. Alsaedi and X. Wang, *Chem. Eng. J.*, 2018, **344**, 380–390.
- W. Xiao, B. Yan, H. Zeng and Q. Liu, *Carbon*, 2016, **105**, 655–664.
- J. A. González, M. E. Villanueva, L. L. Piehl and G. J. Copello, *Chem. Eng. J.*, 2015, **280**, 41–48.
- M. T. Yagub, T. K. Sen, S. Afroze and H. M. Ang, *Adv. Colloid Interface Sci.*, 2014, **209**, 172–184.
- G. Z. Kyzas, D. A. Eleni and M. A. Kostas, *J. Chem. Technol. Biotechnol.*, 2014, **89**, 196–205.
- G. Crini, *Bioresour. Technol.*, 2006, **97**, 1061–1085.
- M. Yusuf, F. M. Elfgi, S. A. Zaidi, E. C. Abdullah and M. A. Khan, *RSC Adv.*, 2015, **5**, 50392–50420.
- K. S. Novoselov, A. K. Geim, S. V. Morozov, D. Jiang, Y. Zhang, S. V. Dubonos, I. V. Grigorieva and A. A. Firsov, *Science*, 2004, **306**, 666–669.
- S. V. Tkachev, E. Y. Buslaeva and S. P. Gubin, *Inorg. Mater.*, 2011, **47**, 1–10.
- S. Stankovich, D. A. Dikin, R. D. Piner, K. A. Kohlhaas, A. Kleinhammes, Y. Jia, Y. Wu, S. T. Nguyen and R. S. Ruoff, *Carbon*, 2007, **45**, 1558–1565.
- Y. Hernandez, M. Lotya, D. Rickard, S. D. Bergin and J. N. Coleman, *Langmuir*, 2010, **26**, 3208–3213.
- A. Y. W. Sham and S. M. Notley, *J. Environ. Chem. Eng.*, 2018, **6**, 495–504.
- P. Montes-Navajas, N. G. Asenjo, R. Santamaria, R. Menendez, A. Corma and H. Garcia, *Langmuir*, 2013, **29**, 13443–13448.
- L. Wu, L. Liu, B. Gao, R. Muñoz-Carpena, M. Zhang, H. Chen, Z. Zhou and H. Wang, *Langmuir*, 2013, **29**, 15174–15181.
- G. Hazell, M. Hinojosa-Navarro, T. M. McCoy, R. F. Tabor and J. Eastoe, *J. Colloid Interface Sci.*, 2016, **464**, 285–290.
- K. W. J. Heard, C. Bartlam, C. D. Williams, J. Zhang, A. A. Alwattar, M. S. Little, A. V. S. Parry, F. M. Porter, M. A. Vincent and I. H. Hiller, *et al.*, *ACS Omega*, 2019, **4**, 1969–1981.
- J. Chen, B. Yao, C. Li and G. Shi, *Carbon*, 2013, **64**, 225–229.
- J. Chen, Y. Li, L. Huang, C. Li and G. Shi, *Carbon*, 2015, **81**, 826–834.
- W. Liu, H. Li, C. Xu, Y. Khatami and K. Banerjee, *Carbon*, 2011, **49**, 4122–4130.
- I. Vlassiuk, P. Fulvio, H. Meyer, N. Lavrik, S. Dai, P. Datskos and S. Smirnov, *Carbon*, 2012, **54**, 58–67.
- W. Yang, G. Chen, Z. Shi, C. Liu, L. Zhang, G. Xie, M. Cheng, D. Wang, R. Yang and D. Shi, *et al.*, *Nat. Mater.*, 2013, **12**, 792–797.
- Y. Hernandez, V. Nicolosi, M. Lotya, F. M. Blighe, Z. Sun, S. De, I. T. McGovern, B. Holland, M. Byrne and Y. K. Gun'Ko, *et al.*, *Nat. Nanotechnol.*, 2008, **3**, 563–568.
- L. Guardia, M. J. Fernández-Merino, J. I. Paredes, P. Solís-Fernández, S. Villar-Rodil, A. Martínez-Alonso and J. M. D. Tascón, *Carbon*, 2011, **49**, 1653–1662.
- S. Sampath, A. N. Basuray, K. J. Hartlieb, T. Aytun, S. I. Stupp and J. F. Stoddart, *Adv. Mater.*, 2013, **25**, 2740–2745.
- R. Narayan, J. Lim, T. Jeon, D. J. Li and S. O. Kim, *Carbon*, 2017, **119**, 555–568.
- N. Liu, F. Luo, H. Wu, Y. Liu, C. Zhang and J. Chen, *Adv. Funct. Mater.*, 2008, **18**, 1518–1525.
- J. Liu, M. Notarianni, G. Will, V. T. Tjong, H. Wang and N. Motta, *Langmuir*, 2013, **29**, 13307–13314.
- A. T. Najafabadi and E. Gyenge, *Carbon*, 2014, **71**, 58–69.
- T. Ardyani, A. Mohamed, S. A. Bakar, M. Sagisaka, Y. Umetsu, M. H. Mamat, M. K. Ahmad, H. P. S. A. Khalil and S. M. King, *et al.*, *Carbohydr. Polym.*, 2020, **228**, 115376.
- K. Parvez, R. Li, S. R. Puniredd, Y. Hernandez, F. Hinkel, S. Wang, X. Feng and K. Müllen, *ACS Nano*, 2013, **7**, 3598–3606.
- J. Gong, X. Gao, M. Li, Q. Nie, W. Pan and R. Liu, *Int. J. Environ. Sci. Technol.*, 2017, **14**, 305–314.

- 35 Z. Xue, S. Zhao, Z. Zhao, P. Li and J. Gao, *J. Mater. Sci.*, 2016, **51**, 4928–4941.
- 36 A. Mohamed, T. Ardyani, S. A. Bakar, M. Sagisaka, Y. Umetsu, M. R. M. Hussin, M. K. Ahmad, M. H. Mamat, S. King and A. Czajka, *et al.*, *Carbohydr. Polym.*, 2018, **201**, 48–59.
- 37 T. Ardyani, A. Mohamed, S. A. Bakar, M. Sagisaka, Y. Umetsu, M. H. Mamat, M. K. Ahmad, H. P. S. A. Khalil, S. King and S. E. Rogers, *et al.*, *J. Colloid Interface Sci.*, 2019, **545**, 184–194.
- 38 L. Zhang, Z. Zhang, C. He, L. Dai, J. Liu and L. Wang, *ACS Nano*, 2014, **8**, 6663–6670.
- 39 A. Mohamed, K. Trickett, S. Y. Chin, S. Cummings, M. Sagisaka, L. Hudson, S. Nave, R. Dyer, S. E. Rogers and R. K. Heenan, *et al.*, *Langmuir*, 2010, **26**, 13861–13866.
- 40 A. Mohamed, A. K. Anas, S. A. Bakar, A. A. Aziz, M. Sagisaka, P. Brown, J. Eastoe, A. Kamari, N. Hashim and I. M. Isa, *Colloid Polym. Sci.*, 2014, **292**, 3013–3023.
- 41 A. B. Suriani, M. D. Nurhafizah, A. Mohamed, A. K. Masrom, V. Sahajwalla and R. K. Joshi, *Mater. Des.*, 2016, **99**, 174–181.
- 42 G. K. Ramesha, A. V. Kumara, H. B. Muralidhara and S. Sampath, *J. Colloid Interface Sci.*, 2011, **361**, 270–277.
- 43 W. Konicki, M. Aleksandrak and E. Mijowska, *Chem. Eng. Res. Des.*, 2017, **123**, 35–49.
- 44 K. Haubner, J. Murawski, P. Olk, L. M. Eng, C. Ziegler, B. Adolph and E. Jaehne, *Chem. Phys. Chem.*, 2010, **11**, 2131–2139.
- 45 Y. Li, Q. Du, T. Liu, X. Peng, J. Wang, J. Sun, Y. Wang, S. Wu, Z. Wang and Y. Xia, *et al.*, *Chem. Eng. Res. Des.*, 2013, **91**, 361–368.
- 46 W. Konicki, M. Aleksandrak, D. Moszyński and E. Mijowska, *J. Colloid Interface Sci.*, 2017, **496**, 188–200.
- 47 K. Y. Foo and B. H. Hameed, *Chem. Eng. J.*, 2010, **156**, 2–10.
- 48 I. Langmuir, *J. Am. Chem. Soc.*, 1918, **40**, 1361–1403.
- 49 H. Freundlich, *J. Phys. Chem. A*, 1906, **57**, 1100–1107.
- 50 J. Zhang, Y. Zhou, M. Jiang, J. Li and J. Sheng, *J. Mol. Liq.*, 2015, **209**, 267–271.
- 51 Y. S. Ho, *J. Hazard. Mater.*, 2006, **136**, 681–689.
- 52 S. Bai, X. Shen, X. Zhong, Y. Liu, G. Zhu, X. Xu and K. Chen, *Carbon*, 2012, **50**, 2337–2346.
- 53 M. Lotya, Y. Hernandez, P. J. King, R. J. Smith, V. Nicolosi, L. S. Karlsson, F. M. Blighe, S. De, Z. Wang and I. T. McGovern, *et al.*, *J. Am. Chem. Soc.*, 2009, **131**, 3611–3620.
- 54 J. N. Coleman, *Adv. Funct. Mater.*, 2009, **19**, 3680–3695.
- 55 A. Mohamed, T. Ardyani, S. A. Bakar, M. Sagisaka, Y. Umetsu, J. J. Hamon, B. A. Rahim, S. R. Esa, H. P. S. A. Khalil and M. H. Mamat, *et al.*, *J. Colloid Interface Sci.*, 2018, **516**, 34–47.
- 56 Y. Hao, Y. Wang, L. Wang, Z. Ni, Z. Wang, R. Wang, C. K. Koo, Z. Shen and J. T. L. Thong, *Small*, 2010, **6**, 195–200.
- 57 C. Soldano, A. Mahmood and E. Dujardin, *Carbon*, 2010, **48**, 2127–2150.
- 58 V. C. Tung, M. J. Allen, Y. Yang and R. B. Kaner, *Nat. Nanotechnol.*, 2009, **4**, 25–29.
- 59 A. C. Ferrari and J. Robertson, *Phys. Rev. B: Condens. Matter Mater. Phys.*, 2001, **64**, 1–13.
- 60 Y. Zhu, S. Murali, W. Cai, X. Li, J. W. Suk, J. R. Potts and R. S. Ruoff, *Adv. Mater.*, 2010, **22**, 3906–3924.
- 61 R. J. Smith, M. Lotya and J. N. Coleman, *New J. Phys.*, 2010, **12**, 125008–125018.
- 62 R. J. Hunter, *Introduction to modern colloid science*, Oxford University Press, 1993.
- 63 J. N. Israelachvili, *Intermolecular and surface forces*, Academic Press, 2011, vol. 59.
- 64 D. W. Johnson, B. P. Dobson and K. S. Coleman, *Curr. Opin. Colloid Interface Sci.*, 2015, **20**, 367–382.
- 65 D. Li, M. B. Müller, S. Gilje, R. B. Kaner and G. G. Wallace, *Nat. Nanotechnol.*, 2008, **3**, 101–105.
- 66 Z. Sun, V. Nicolosi, D. Rickard, S. D. Bergin, D. Aherne and J. N. Coleman, *J. Phys. Chem. C*, 2008, **112**, 10692–10699.
- 67 F. Zhang, S. Li, Q. Zhang, J. Liu, S. Zeng, M. Liu and D. Sun, *J. Mol. Liq.*, 2019, **276**, 338–346.
- 68 F. Baskoro, C. Wong, S. R. Kumar, C. Chang, C. Chen, D. W. Chen and S. J. Lue, *J. Membr. Sci.*, 2018, **554**, 253–263.
- 69 Y. Si and E. T. Samulski, *Nano Lett.*, 2008, **8**, 1679–1682.
- 70 J. Eastoe, A. Paul, A. Downer, D. C. Steytler and E. Rumsey, *Langmuir*, 2002, **7**, 3014–3017.
- 71 S. Gold, J. Eastoe, R. Grilli and D. C. Steytler, *Colloid Polym. Sci.*, 2006, **284**, 1333–1337.
- 72 M. J. Rosen, *Surfactants and interfacial phenomena*, John Wiley & Sons Inc., New York, 2004.
- 73 D. Myers, *Surfactant science and technology*, John Wiley & Sons, Inc., Hoboken, New Jersey, 2005.
- 74 A. Mohamed, M. Sagisaka, M. Hollamby, S. E. Rogers, R. K. Heenan, R. Dyer and J. Eastoe, *Langmuir*, 2012, **28**, 6299–6306.
- 75 A. Czajka, G. Hazell and J. Eastoe, *Langmuir*, 2015, **31**, 8205–8217.
- 76 M. T. Stone, P. G. Smith, S. R. P. Rocha, P. J. Rossky and K. P. Johnston, *J. Phys. Chem. B*, 2004, **108**, 1962–1966.
- 77 T. M. McCoy, L. De Campo, A. V. Sokolova, I. Grillo, E. I. Izgorodina and R. F. Tabor, *Phys. Chem. Chem. Phys.*, 2018, **20**, 16801–16816.
- 78 D. C. Marcano, D. V. Kosynkin, J. M. Berlin, A. Sinitskii, Z. Sun, A. Slesarev, L. B. Alemany, W. Lu and J. M. Tour, *ACS Nano*, 2010, **4**, 4806–4814.
- 79 K. Krishnamoorthy, M. Veerapandian, K. Yun and S. J. Kim, *Carbon*, 2013, **53**, 38–49.
- 80 A. M. Abdelkader, A. J. Cooper, R. A. W. Dryfe and I. A. Kinloch, *Nanoscale*, 2015, **7**, 6944–6956.
- 81 P. Li, S. H. Bae, Q. Y. Zan, N. H. Kim and J. H. Lee, *Adv. Mater. Res.*, 2010, **123–125**, 743–746.